Bulletin of the Seismological Society of America, Vol. 99, No. 2A, pp. 876–883, April 2009, doi: 10.1785/0120080008

Short Note

Fault Slip Velocities Inferred from the Spectra of Ground Motions

by N. Ani Anil-Bayrak and Igor A. Beresnev

Abstract There is much practical need in obtaining independent information about earthquake-source dynamic properties directly from observable data. One such dynamic parameter, the peak slip velocity during earthquake rupture, can be calculated from the corner frequencies of the source spectra, on the assumption of the validity of the ω^2-source model. To obtain the source terms, observed Fourier spectra should be corrected for the site and path effects. Small-to-moderate earthquakes in Japan recorded on multiple rock sites are well suited for the application of this methodology. The results indicate that the maximum slip velocity of the selected earthquakes ranged from approximately 0.2 to 0.6 m/sec. Direct observation-based determinations of this type provide valuable physical information about the in-situ faulting processes that can be used for constraining dynamics theories of faulting or in ground-motion prediction.

Introduction

Observations constraining dynamic parameters of rupturing faults are important for understanding the physics of the processes in the earthquake source. Such observations come from the interpretation of recorded data, for example, of the Fourier spectra of ground-motion accelerograms, provided characteristics of such spectra can be linked to a particular dynamic-source parameter.

Beresnev (2001, 2002) and Beresnev and Atkinson (2002) argued that, theoretically, the maximum slip velocity on a rupturing fault is the source parameter controlling the fault's high-frequency radiation, thus determining the level of seismic hazard. It has also been recently suggested that the peak slip velocity may place an upper bound on the peak ground motion experienced during an earthquake (McGarr and Fletcher, 2007). This dynamic-source parameter, therefore, acquires substantial practical meaning.

Beresnev (2001, 2002) and Beresnev and Atkinson (2002) provided the framework from which this parameter can be directly calculated from the corner frequencies of the shear-wave spectra. This framework is based upon the fact that earthquakes, at least of small-to-moderate size, typically radiate the particle-acceleration Fourier spectra in the far field that follow the ω^2 shape,

$$u_{\mathrm{FF}}(\omega) = CM_0\omega^2[1 + (\omega/\omega_c)^2]^{-1}, \tag{1}$$

where C is a constant, M_0 is the seismic moment, and ω_c is the spectrum's corner frequency (e.g., Boore, 1983). The functional form of the shear-dislocation displacement time history that radiates this spectrum is

$$u(t) = U[1 - (1 + t/\tau)\exp(-t/\tau)], \tag{2}$$

where U is the dislocation's final displacement and $\tau \equiv 1/\omega_c$. The maximum value $v_{\max}$ of the slip velocity $u'(t)$ is

$$v_{\max} = \omega_c U/e, \tag{3}$$

where e is the base of the natural logarithm. Using the definition of the seismic moment, $M_0 = \mu UA$, where μ is the shear modulus and A is the rupture area, and the relationship $V_S = (\mu/\rho)^{1/2}$, where V_S is the shear-wave velocity and ρ is the density, one finally renders (3) in the form

$$v_{\max} = (2\pi/e)(M_0/\rho V_S^2 A) f_c, \tag{4}$$

where $f_c = \omega_c/2\pi$ (equation 7 in Beresnev, 2002). Equation (4) allows estimation of the maximum slip velocity from the corner frequency and the other observable data.

The corner frequencies are picked from the source spectra, which, therefore, should be separated from the distorting path and site effects. A common model of a recorded spectrum is

$$\text{recorded spectrum}\,(R, f) = \text{source}\,(f) \times \text{path}\,(R, f) \times \text{site}\,(f), \tag{5}$$

where R is the distance to the observation point. The term source (f) is represented by equation (1). The path effect is typically approximated as

$$\text{path}\,(R, f) = \frac{\exp[-\pi f R/Q(f)V_S]}{R/R_0}, \qquad (6)$$

where R_0 is a reference distance and $Q(f)$ is the quality factor characterizing anelastic attenuation. Assuming a hard-rock site condition (no significant local response), the site effect can be written as

$$\text{site}\,(f) = \text{crustal amplification}\,(f)\exp(-\pi\kappa f), \qquad (7)$$

where the Anderson–Hough kappa (κ) describes the high-frequency spectral rolloff.

Isolating the source term from the path and site effects within model (5) has been performed in a variety of studies (e.g., Prejean and Ellsworth, 2001; Chen and Atkinson, 2002; Ottemöller and Havskov, 2003). In our work, the approach exemplified by equations (4)–(7) will be applied to isolating the source spectra and determining the corner frequencies and maximum slip velocities on faults during earthquakes. The assumption of a single-corner spectrum requires treating earthquakes as point sources (e.g., Savage, 1972); to that end, small-to-moderate-magnitude events will be used. To avoid complications related to the specifics of a local shallow-soil response, the analysis will deal with rock sites, for which straightforward crustal-amplification models can be used.

Data Description

We applied the technique to high-quality digital data recorded on rock sites by the KiK-Net strong-motion network in Japan. We considered the events in the magnitude range from 4 to 6 available through the KiK-Net online database (see the Data and Resources section). The Web site provides downhole and surface acceleration records for all three components of the strong-motion data. The accelerometers have a flat response from 0.1 Hz to the cutoff frequency of 30 Hz (see the Data and Resources section). The sampling rate is 200 Hz. To minimize the effect of near-surface weathering and noise on the records, the data from the downhole accelerometers were used.

From this event group, we selected the earthquakes (1) that produced recordings at at least two different rock sites and (2) whose spectra followed the assumed ω^2 shape. The former criterion is needed to estimate a possible variability in the corner frequencies depending on the azimuth from the source to the recording site. The latter retains the validity of the underlying spectral model (1); although the ω^2 model is widely observed and used in seismology, there is no reason to believe that a variety of source processes will be exhausted by this only possibility.

Five earthquakes fit these criteria, whose parameters are listed in Table 1 along with the rock stations that recorded them. The station parameters with the geology are tabulated in Table 2, and the locations of both the earthquakes and the stations are shown in Figure 1. The lithology listed refers to the downhole accelerometer; to maximize the number of records, we have included all stations with the hard-rock condition downhole, even if a soil layer was present at the surface (Anil Bayrak, 2008, figure 2-1).

Data Processing and Corrections

All three components (east–west [EW], north–south [NS], and up–down [UD]) of the records were used to determine the shear-wave window, with its maximum length set to 10 sec (see example in Fig. 2). The window was cosine-tapered at the ends at 5% of its length, and its Fourier amplitude spectrum was computed. Proper care was exercised

Table 1
Earthquake and Station Information

Date (yyyy/mm/dd)	Time (hh:mm UTC)	Latitude (°)	Longitude (°)	Magnitude*	Moment Magnitude	Depth (km)	Stations	Hypocentral Distance (km)
2006/05/28	20:36	33.339	131.799	4.3	4.2	80	YMGH02	131
							YMGH04	113
							YMGH11	126
2006/07/11	03:09	34.022	131.169	4.0	3.9	16	FKOH03	78
							FKOH04	67
							YMGH08	29
2007/01/22	02:16	35.730	136.340	4.5	4.5	13	GIFH07	38
							NARH06	125
2007/04/26	09:03	33.885	133.586	5.3	5.3	39	EHMH03	40
							HRSH01	84
							OKYH02	113
							OKYH07	137
							OKYH09	149
							OKYH11	146
2007/05/13	08:14	35.005	132.795	4.6	4.6	9	HRSH07	82
							OKYH04	92
							YMGH02	181
							YMGH04	128

*JMA magnitude.

Table 2
Rock Sites that Recorded the Events Selected

Site Code	Latitude (°)	Longitude (°)	Depth (m)	Geology
EHMH03	33.9121	133.6523	100	Black Schist
FKOH03	33.5575	130.5522	100	Granite
FKOH04	33.5479	130.7475	100	Granodiorite
GIFH07	35.4147	136.4376	100	Slate
HRSH01	34.3701	133.0259	205	Orthoclase Biotite Granite
HRSH07	34.2850	132.6436	102	Granite
NARH06	34.6381	136.0540	101	Granite, Granodiorite
OKYH02	34.7468	134.0728	200	Granite
OKYH04	34.6397	133.6888	100	Granite
OKYH07	35.0461	133.3196	100	Granite
OKYH09	35.1777	133.6792	100	Granite
OKYH11	35.0700	134.1189	200	Slate
YMGH02	34.1078	131.1458	200	Sandstone, Granodiorite
YMGH04	34.0237	132.0651	100	Granite
YMGH11	34.2058	131.6883	200	Granite

as to not make the 5% taper affect the shear-wave arrival. The spectra of EW and NS components were arithmetically averaged. Figure 3 shows the horizontal-component spectra of the shear-wave window shown in Figure 2, and their average is presented in Figure 4. As exemplified earlier in equation (5), the recorded spectrum is formed from three components: the source spectrum, the path effect, and the site effect. The path and site effects were separated from the recorded spectra, and the obtained source spectrum was used to identify the corner frequencies.

Path-Effect Corrections

Equation (6) was applied to remove the path effect. We follow Chen and Atkinson (2002, pp. 887–888) in using Japan's geometric spreading factor of R^{-1} appearing in equation (6). However, in our specific study, aimed at identifying the corner frequencies of the source spectra, the choice of an exact form of the spreading is not important. Because the latter is frequency independent, it just scales the spectrum by a constant value and does not affect the position of the corner frequency.

The earthquakes found occurred over a large area, and there is no region-specific quality factor $Q(f)$ available for each event–station pair. We therefore used, as the best approximation, two different quality factors available from the literature: one for the Kanto region (Kinoshita, 1994; also used for the entire region of Japan by Chen and Atkinson, 2002, table 3),

$$Q(f) = 130f^{0.7} \qquad (f = 0.5\text{–}16 \text{ Hz}), \tag{8}$$

Figure 1. Earthquakes (stars) and stations (balloons) used in this study.

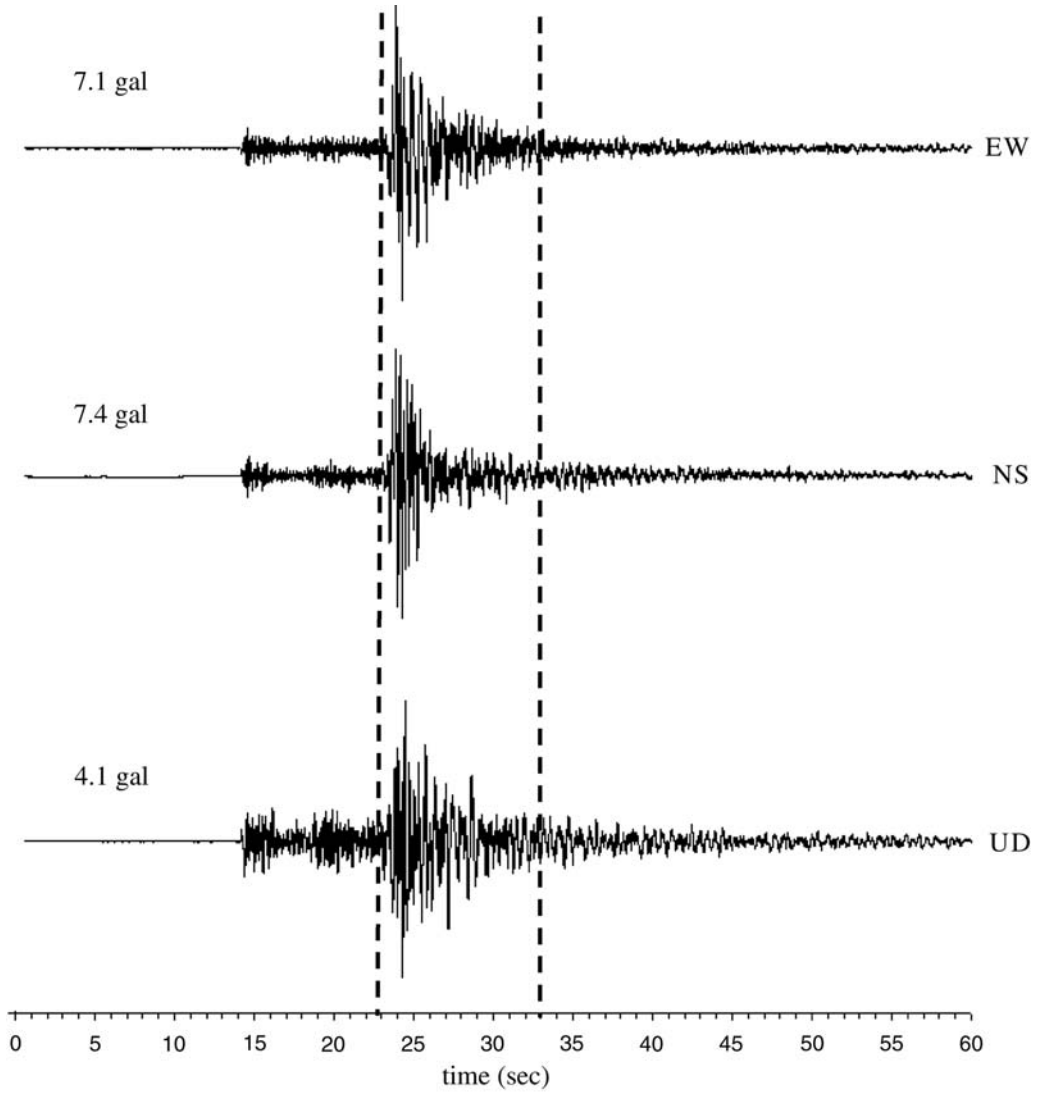

Figure 2. Three components of acceleration data and the shear-wave window selected for the calculations. This example is the data recorded at station HRSH01 during the 26 April 2007 earthquake.

and the other for the Kinki region (Petukhin *et al.*, 2003),

$$Q(f) = 180f^{0.7} \qquad (f = 1\text{–}35 \text{ Hz}). \tag{9}$$

Figure 5 shows the geographic position of these regions relative to the earthquake epicenters; they all belong to the central and southwestern Japan. The equal frequency dependence in equations (8) and (9) supports the consistency in the regional Q determinations. Spectral fitting outside the range of the approximate validity of these combined attenuation laws was not attempted. We will later analyze possible uncertainties associated with the different scaling coefficients in (8) and (9).

Another parameter for the path-effect calculation is the crustal shear-wave velocity. We assumed $V_S = 3.6$ km/sec, following Chen and Atkinson who used this value for Japan. The reference distance was 1 km.

Site-Effect Corrections

The site-effect correction was applied according to equation (7). From the comparison of large quantities of recorded data, Chen and Atkinson (2002) reached a conclusion that generic crustal amplifications for California and Japan rock and shallow-soil sites appeared to have the same shape; this allowed us to use the generic rock-amplification model developed for western North America by Boore and Joyner (1997, table 3). Because this model provides amplifications for the specific frequencies, amplifications for other frequencies were calculated by interpolation. The Japan kappa of $\kappa = 0.035$ sec in equation (7) was also as in Chen and Atkinson (2002, table 3).

As an example of the application of this procedure, Figure 6 shows the spectrum from Figure 4 after the path- and site-effect corrections have been applied. Based on the signal-to-noise ratio analysis of Beresnev *et al.* (2002) and

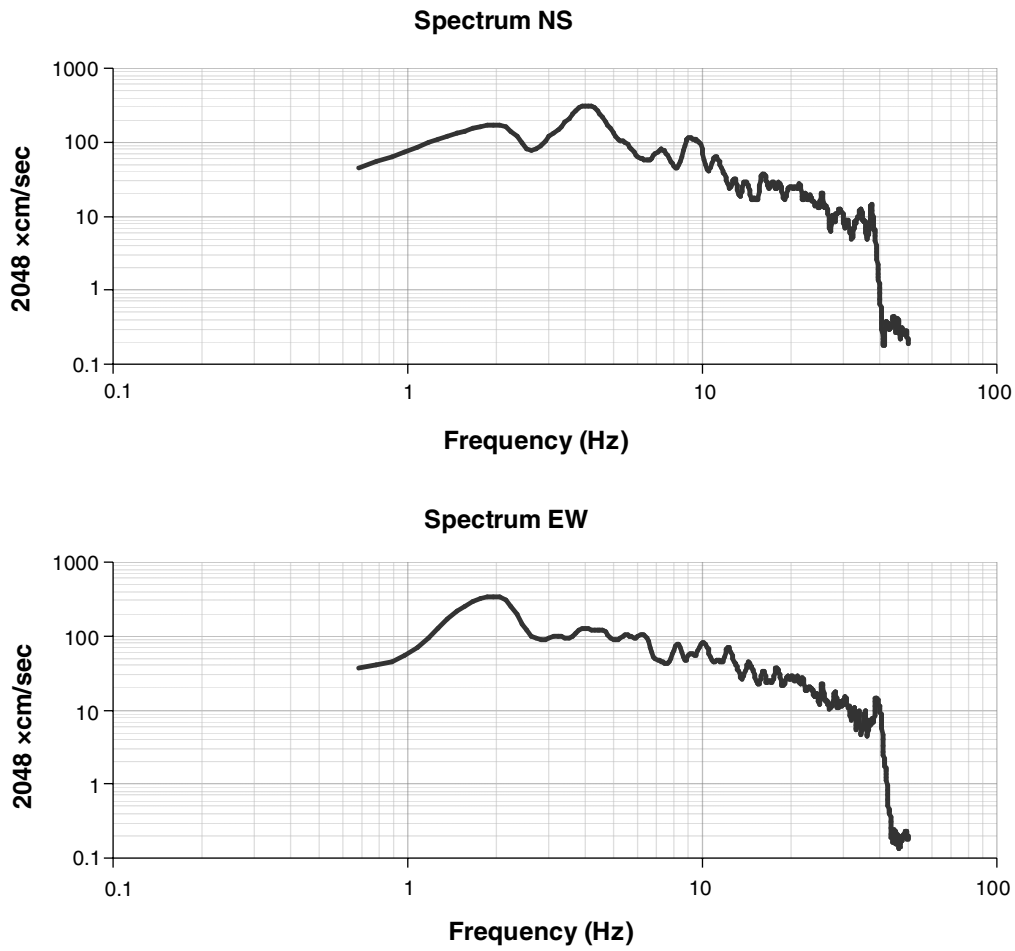

Figure 3. Raw Fourier spectra of the horizontal components of the shear-wave window shown in Figure 2.

the frequency-range applicability of the attenuation laws (8) and (9), the analysis was performed for the frequencies above 0.5 Hz. Two different slopes can clearly be seen. Following Savage (1972), the corner frequency f_c is found as the intersection of the linear fits to the slopes. Equation (4) then allows calculation of the maximum slip velocity by using the corner frequency and the other observable data.

Note that we prefer to use the most direct, graphical, method of the corner-frequency determination, based on the definition. Alternatively, the corner frequency can be ob-

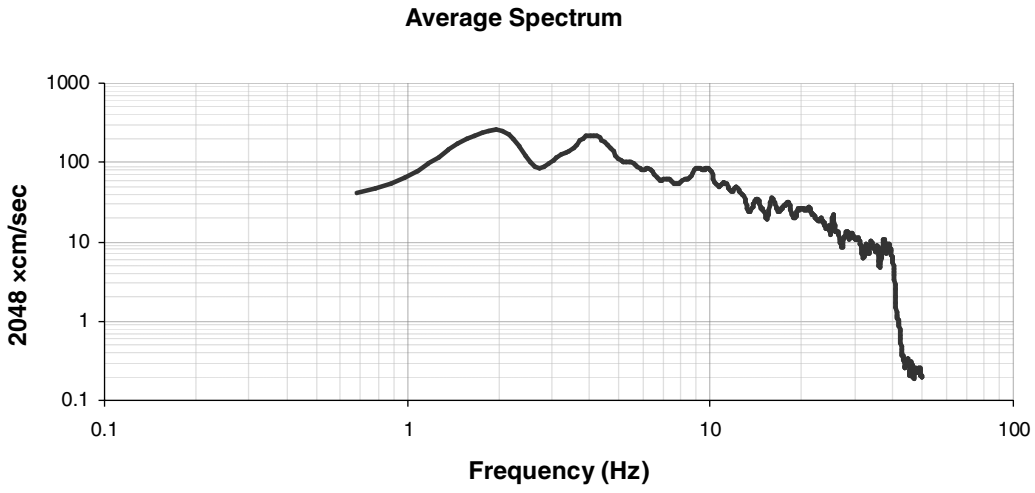

Figure 4. The averaged spectrum of the spectra shown in Figure 3.

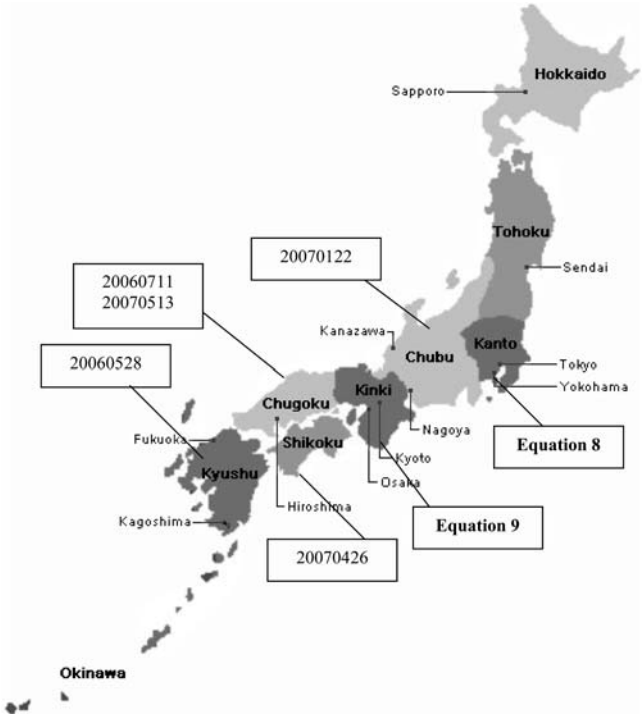

Figure 5. The earthquakes and $Q(f)$-values.

tained from matching the entire theoretical source spectrum (1) or its high-frequency asymptote. There are significant caveats to this alternative method, though, in our opinion. An accurate calculation would require exact knowledge of M_0 and the coefficient C, which involves the values of V_S, ρ, and the source radiation pattern (e.g., Boore, 1983, equation 2). The values of these seismological parameters typically come with significant (and usually unknown) uncertainties, which would map, along with the error in the determination of the spectral slopes, into the calculation of the corner frequency. Estimates show that an uncertainty of a factor of two in the resulting f_c can easily be obtained. In our view, it is reasonable to avoid this propagation of error by using the direct graphical method, which, all other factors being equal, will only incorporate the uncertainty in the determination of the slopes among all the uncertainties of the input parameters mentioned. It should be acknowledged, though, that both methods are not free of irreducible uncertainties, and that they will generally return different results. Both corner frequencies and, hence, slip velocities cannot be determined with easily quantifiable precision—unless a large number of consistent observations are available, which is seldom the case. The following results in Table 3 should be viewed with these cautions in mind.

It also should be noted that, although borehole recordings on rock sites were used, local amplifications cannot be entirely ruled out; this is why we apply the station-averaging procedure. For example, the peak exhibited by the spectrum in Figure 6 at the very end of the high-frequency range may be due to a local response.

Equation (4) includes M_0, which can be calculated from the empirical formula for moderate earthquakes (Moya *et al.*, 2000):

$$\log M_0 = 1.54 M_{\mathrm{JMA}} + 15.8, \tag{10}$$

where M_{JMA} is the Japan Meteorological Agency (JMA) magnitude appearing in Table 1 and M_0 is in dyne centimeter. The density in (4) was taken as $\rho = 2.8$ g/cm^3 (Chen and Atkinson, 2002). Following Beresnev and Atkinson (2002), the rupture area was determined through the Wells and Coppersmith (1994, table 2A and fig. 16a) empirical formula:

$$\log A = -3.49 + 0.91 M, \tag{11}$$

where M is the moment magnitude and A is in km^2. The magnitude M was obtained from M_0 using the definition

$$M = \frac{2}{3}\log M_0 - 10.7, \tag{12}$$

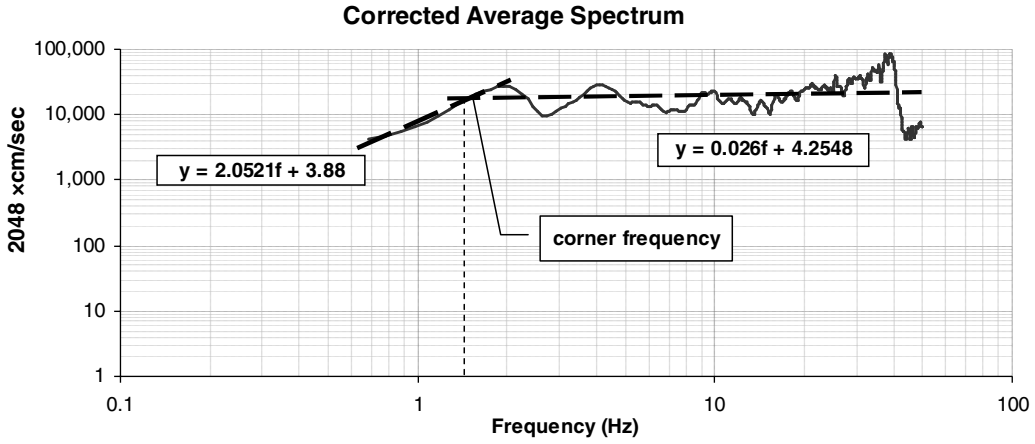

Figure 6. The spectrum from Figure 4 corrected for the path and site effects. The corner frequency and the fitted lines (dashed lines) are shown.

Table 3
Corner Frequencies and Maximum Slip Velocities for Different Choices of Q

	$Q(f) = 130f^{0.7}$		$Q(f) = 180f^{0.7}$			
Earthquake	Mean Corner Frequency (Hz)	Mean Maximum Slip Velocity (cm/sec)	Mean Corner Frequency (Hz)	Mean Maximum Slip Velocity (cm/sec)	Standard Deviation of Corner Frequency (Hz)	Standard Deviation of Maximum Slip Velocity (cm/sec)
2006/05/28	2.6	20	2.7	21	0.5	4
2006/07/11	3.4	17	3.6	18	0.3	2
2007/01/22	1.9	19	2.0	20	—	—
2007/04/26	1.9	56	1.9	59	0.5	15
2007/05/13	1.6	18	1.6	18	0.2	2

where M_0 is in dyne centimeter (Hanks and Kanamori, 1979). The moment magnitude, converted from M_{JMA} using relations (10) and (12), is also listed in Table 1. The difference is insignificant.

Results and Summary

Table 3 summarizes the calculated corner frequencies and peak slip velocities for the five earthquakes. Two different source spectra were obtained corresponding to the two $Q(f)$ models (equations 8 and 9). It is seen that the respective corner frequencies and slip velocities are very close to each other. The standard deviations in the corner frequency, resulting from its variability depending on the azimuth to the station, along with the ensuing standard deviation in the determination of the slip velocity, are also listed for $Q(f) = 180f^{0.7}$. The number of readings used to calculate the standard deviation is the same as the number of stations in Table 1.

The maximum slip velocities calculated for these small and moderate earthquakes range between approximately 0.2 and 0.6 m/sec. It is interesting to compare these values with those available from independent studies of other events. Rice (2007) and Brown *et al.* (2007) reported the typical seismic slip rates in the range of 0.1–0.8 and 0.5–2 m/sec, respectively. Kanamori (1972) and Abe (1974) resolve slip-velocity values of 0.4 and 0.5 m/sec, respectively. All these values are fully compatible with our direct measurements. On the other hand, McGarr and Fletcher (2007) summarized peak slip velocities for eight large earthquakes from different world regions ranging from 2.3 to 12 m/sec. The discrepancy with our results is obvious, in that their values are systematically larger. In interpreting the determinations by McGarr and Fletcher, it should be kept in mind, though, that all of them have been obtained from published finite-fault slip inversions and not directly from ground-motion records. There are reasons to believe that such inversions are not necessarily reliable and should be interpreted with much caution; there is presently no established way of assessing their quality (see Beresnev, 2003, for a review). In our opinion, the more-direct determinations should be preferred.

The direct method for peak-slip-velocity calculation that we have tested provides valuable independent information for the studies of the in-situ dynamic fault properties and supplies further observational constraints for the development of the theories of dynamic faulting.

Data and Resources

The accelerographic data from the KiK-Net network were searched through the Web site www.kik.bosai.go.jp (last accessed August 2008). To view the characteristics of the accelerometers, see www.kik.bosai.go.jp/kik/ftppub/seismo/KiK_characteristics.png (last accessed August 2008).

Acknowledgments

This study was partially supported by Iowa State University. We are grateful to G. Atkinson, J. Fletcher, and an anonymous referee for the valuable suggestions.

References

Abe, K. (1974). Seismic displacement and ground motion near a fault: the Saitama earthquake of September 21, 1931, *J. Geophys. Res.* **79,** 4393–4399.

Anil Bayrak, N. A. (2008). Fault slip velocities inferred from the spectra of ground motion, *Master's Thesis*, Iowa State University.

Beresnev, I. A. (2001). What we can and cannot learn about earthquake sources from the spectra of seismic waves, *Bull. Seismol. Soc. Am.* **91,** 397–400.

Beresnev, I. A. (2002). Source parameters observable from the corner frequency of earthquake spectra, *Bull. Seismol. Soc. Am.* **92,** 2047–2048.

Beresnev, I. A. (2003). Uncertainties in finite-fault slip inversions: to what extent to believe? (A critical review), *Bull. Seismol. Soc. Am.* **93,** 2445–2458.

Beresnev, I. A., and G. M. Atkinson (2002). Source parameters of earthquakes in eastern and western North America based on finite-fault modeling, *Bull. Seismol. Soc. Am.* **92,** 695–710.

Beresnev, I. A., A. M. Nightengale, and W. J. Silva (2002). Properties of vertical ground motions, *Bull. Seismol. Soc. Am.* **92,** 3152–3164.

Boore, D. M. (1983). Stochastic simulation of high-frequency ground motions based on seismological models of the radiated spectra, *Bull. Seismol. Soc. Am.* **73,** 1865–1894.

Boore, D., and W. Joyner (1997). Site amplifications for generic rock sites, *Bull. Seismol. Soc. Am.* **87,** 327–341.

Brown, K. M., Y. Fialko, and C. Hartsig (2007). Complex evolution of friction during seismic slip: new experimental results (Abstract S11E-02), *EOS Trans. AGU* **88,** S11E-02.

Chen, S.-Z., and G. M. Atkinson (2002). Global comparisons of earthquake source spectra, *Bull. Seismol. Soc. Am.* **92,** 885–895.

Hanks, T. C., and H. Kanamori (1979). A moment magnitude scale, *J. Geophys. Res.* **84,** 2348–2350.

Kanamori, H. (1972). Determination of effective tectonic stress associated with earthquake faulting. The Tottori earthquake of 1943, *Phys. Earth Planet. Interiors* **5,** 426–434.

Kinoshita, S. (1994). Frequency-dependent attenuation of shear waves in the crust of the southern Kanto area, Japan, *Bull. Seismol. Soc. Am.* **84,** 1387–1396.

McGarr, A., and J. B. Fletcher (2007). Near-fault peak ground velocity from earthquake and laboratory data, *Bull. Seismol. Soc. Am.* **97,** 1502–1510.

Moya, A., J. Aguirre, and K. Irikura (2000). Inversion of source parameters and site effects from strong ground motion records using genetic algorithms, *Bull. Seismol. Soc. Am.* **90,** 977–992.

Ottemöller, L., and J. Havskov (2003). Moment magnitude determination for local and regional earthquakes based on source spectra, *Bull. Seismol. Soc. Am.* **93,** 203–214.

Petukhin, A., K. Irikura, S. Ohmi, and T. Kagawa (2003). Estimation of *Q*-values in the seismogenic and aseismic layers in the Kinki Region, Japan, by elimination of the geometrical spreading effect using ray approximation, *Bull. Seismol. Soc. Am.* **93,** 1498–1515.

Prejean, S. G., and W. L. Ellsworth (2001). Observations of earthquake source parameters at 2 km depth in the Long Valley caldera, eastern California, *Bull. Seismol. Soc. Am.* **91,** 165–177.

Rice, J. R. (2007). Heating and weakening of major faults during seismic rupture (Abstract S11E-01), *EOS Trans. AGU* **88,** S11E-01.

Savage, J. C. (1972). Relation of corner frequency to fault dimensions, *J. Geophys. Res.* **77,** 3788–3795.

Wells, D. L., and K. J. Coppersmith (1994). New empirical relationships among magnitude, rupture length, rupture width, rupture area, and surface displacement, *Bull. Seismol. Soc. Am.* **84,** 974–1002.

Department of Geological and Atmospheric Sciences
Iowa State University
253 Science I
Ames, Iowa 50011-3212
ani@iastate.edu
beresnev@iastate.edu

Manuscript received 1 April 2008